

Short communication

Correlations between tissue-level stresses and strains and cellular damage within the guinea pig spinal cord white matter

Beth Galle^a, Hui Ouyang^b, Riyi Shi^{b,c}, Eric Nauman^{a,c,*}

^a*School of Mechanical Engineering, Purdue University, 585 Purdue Mall, West Lafayette, IN 47907, USA*

^b*Department of Basic Medical Sciences, Purdue University, West Lafayette, IN 47907, USA*

^c*Weldon School of Biomedical Engineering, Purdue University, West Lafayette, IN 47907, USA*

Accepted 14 March 2007

Abstract

Strain magnitude, strain rate, axon location, axon size, and the local tissue stress state have been proposed as the mechanisms governing primary cellular damage within the spinal cord parenchyma during slow compression injury. However, the mechanism of axon injury has yet to be fully elucidated. The objective of this study was to correlate cellular damage within the guinea pig spinal cord white matter, quantified by a horseradish peroxidase (HRP) exclusion test, with tissue-level stresses and strains using a combined experimental and computational approach. Force–deformation curves were acquired by transversely compressing strips of guinea pig spinal cord white matter at a quasi-static rate. Hyperelastic material parameters, derived from a Mooney–Rivlin constitutive law, were varied within a nonlinear, plane strain finite element model of the white matter strips until the computational force–deformation curve converged to the experimental results. In addition, white matter strips were subjected to nominal compression levels of 25%, 50%, 70%, and 90% to assess axonal damage by quantifying HRP uptake. HRP uptake density increased with tissue depth and with increased nominal compression. Using linear and nonlinear regression analyses, the strongest correlations with HRP uptake density were found for groups of tissue-level stresses and groups of log-transformed tissue-level strains.

© 2007 Elsevier Ltd. All rights reserved.

Keywords: Spinal cord injury; Finite element analysis; Mooney–Rivlin constitutive law; Computational modeling; HRP exclusion assay

1. Introduction

Slow compression spinal cord injuries result from degenerative, infective, or oncologic lesion growths within the spinal canal; the narrowed spinal canal exerts pressure throughout the entire spinal cord parenchyma, resulting in white matter cellular damage. Neurological deficits appear when the spinal cord cross-sectional area is reduced by 30% and are irreversible when cord area reduction exceeds 65% (Fehlings and Skaf, 1998). White matter cellular damage has been theorized to be a function of axon cross-sectional area (Kraus, 1996), tissue strain and strain rate

(Shi and Whitebone, 2006), or tissue stress state (Henderson et al., 2005).

The objectives of this study were first, to characterize the mechanical response of spinal cord white matter with hyperelastic material parameters and second, to quantitatively establish a link between tissue-level stresses and strains invoked during slow compression and white matter cellular injury.

2. Methods

2.1. Tissue acquisition

The dissection procedure used to excise guinea pig spinal cords has been described previously and was approved by the Purdue University Animal Care and Use Committee (Shi and Blight, 1996; Shi and Pryor, 2002; Shi and Whitebone, 2006). Adult guinea pigs were used in this study

*Corresponding author. School of Mechanical Engineering, Purdue University, 585 Purdue Mall, West Lafayette, IN 47907, USA.

Tel.: +1 765 494 8602; fax: +1 765 494 0539.

E-mail address: enauman@purdue.edu (E. Nauman).

(body weight: 255–350 g). Following animal sacrifice, spinal cords were removed and dissected to isolate strips of white matter.

2.2. Transverse compression of white matter strips

Tissue specimens ($n = 7$), at room temperature, were deformed at 0.05 mm/s to 90% nominal transverse compression. Compression followed five preconditioning cycles to 3% nominal compression and a subsequent 30 s dwell interval. A high-resolution electromechanical linear actuator (model LTA-HS, Newport Corporation, Irvine, CA) applied the tissue deformation and was controlled by a single-axis controller (model ESP 100, Newport Corporation) interfaced with LabView. Force feedback was measured by a 1000 g load cell (model 31, Sensotec, Columbus, OH) throughout the loading protocol (sampling rate: 16 Hz). Digital photographs were taken throughout compression to monitor tissue deformation.

2.3. Quantification of axonal damage

The horseradish peroxidase (HRP) exclusion test used to quantify axonal damage has been described previously (Shi, 2004; Shi and Borgens, 2000; Shi and Pryor, 2002; Shi and Whitebone, 2006). Permeabilized axons within each of three tissue regions (Fig. 2) were counted and normalized by the cross-sectional area of the region to obtain HRP uptake density.

The medial, intermediate, and lateral (M, I, and L) tissue regions were located directly beneath the tissue indenter, consistent with previous work (Shi and Borgens, 2000). HRP uptake density was quantified at each of four levels of nominal compression: 25% ($n = 5$), 50% ($n = 5$), 70% ($n = 6$), and 90% ($n = 5$).

2.4. Guinea pig white matter FEM

A two-dimensional, hyperelastic, finite deformation, plane strain FEM of the guinea pig white matter was developed to mimic the experimental protocol (software: COMSOL 3.2 with MATLAB). The hyperelastic constitutive relation used to describe the tissue response was derived from the Mooney–Rivlin strain energy function, W :

$$W = C_{10}(I_1 - 3) + C_{01}(I_2 - 3), \quad (1)$$

where C_{10} and C_{01} are material parameters and I_1 and I_2 are invariants of the right Cauchy–Green deformation tensor.

Using a parametric, nonlinear analysis, the white matter FEM was deformed in increments of 5% nominal compression. The penalty-barrier method was used to model *in vitro* contact between the tissue and the impinging indenter. The contact force exponentially increased as the distance between the tissue and the indenter decreased. The contact force was integrated at each deformation step to obtain the total applied force, thereby generating force–deformation curves.

An iteration scheme, utilizing the MATLAB function `fminsearch`, varied material parameters C_{10} and C_{01} until the computational force–deformation response converged to each of the seven experimental force–deformation curves (Fig. 2). Goodness of fit was quantified by the RMS error between computational and experimental curves. Principal, normal, and shear stresses and strains, von Mises stresses, and strain energy densities were averaged within each region of the tissue for each of the seven computational models.

2.5. Statistical analysis

HRP uptake densities for nominal transverse tissue compression levels of 25%, 50%, 70%, and 90% were compared using an analysis of variance (ANOVA) with a Student–Newman–Keuls post hoc test (Glantz, 2002). HRP uptake densities were then correlated with the average stress and strain measures within each region of the computational model using single and multiple regression analyses for nominal transverse tissue compression levels of 25%, 50%, and 70%. To investigate the possibility of a nonlinear relationship between strain and HRP uptake density, we

assumed a relationship of the form (Barenblatt, 1996):

$$\Pi_1^{\alpha_1} \Pi_2^{\alpha_2} \dots \Pi_N^{\alpha_N} = A \Phi^\beta, \quad (2)$$

where the Π_i terms were principal and normal strains and Φ was the HRP uptake density divided by the HRP uptake density for a transected spinal cord, 4300 axons/mm² (Shi and Borgens, 2000). Linear regression analyses were performed on the log-transformed equations:

$$\alpha_1 \ln \Pi_1 + \alpha_2 \ln \Pi_2 + \dots + \alpha_N \ln \Pi_N = \ln A + \beta \ln \Phi. \quad (3)$$

A significance level of $p < 0.05$ was enforced for all analyses (software: StatView).

3. Results

White matter strip cross-sectional area decreased linearly with increased nominal transverse compression (Fig. 1). The force–deformation responses of the white matter strips (Fig. 2) included an initial toe region where there was no measurable resistance to the applied deformation. Following the toe region, the tissue resistance to additional deformation rapidly increased. The average force magnitude required to achieve 90% nominal transverse compression was 0.246 N (standard deviation: 0.145 N).

HRP uptake density increased with tissue depth and with increased compression (Table 1). For control specimens ($n = 6$), average HRP uptake density was 7.50 axons/mm² (standard deviation: 5.01). All groups statistically differed from the control, with the exception of 25% nominal transverse compression of the intermediate region.

FEMs generated for each experimental force–deformation curve converged to an average of 84.9% nominal transverse compression (standard deviation: 2.58%). The average RMS value of the absolute value of the error between experimental and computational force–deformation curves was 0.0122 N (range: 0.0065–0.0166 N, standard deviation: 0.0034 N). Model parameters C_{10} and C_{01} were found to be 592 ± 323 and 249 ± 45.1 Pa, respectively (means \pm standard deviations).

Single regression analyses demonstrated that HRP uptake density significantly correlated with strain energy density (Table 1). Multiple regression analyses yielded significant correlations between HRP uptake density and groups of stresses. The combination of normal stresses σ_x , σ_y , and σ_z and shear stress τ_{xy} yielded the strongest linear correlation with HRP uptake density. Log-transformed strains were significantly correlated with percent HRP uptake density (Table 2); the strongest correlation was observed for the combination of ε_x , ε_y , and ε_{xy} in-plane strains (Table 3).

4. Discussion

This study is the first to report material parameters of the spinal cord parenchyma in transverse compression. The nonlinear force–deformation response obtained experimentally for the inhomogeneous guinea pig spinal cord white matter strips necessitated the use of a hyperelastic constitutive relation to model the tissue's elastic response.

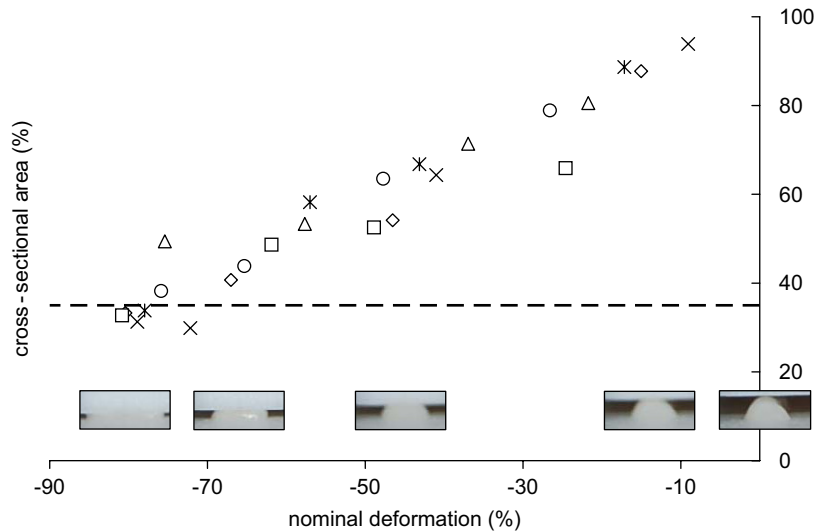


Fig. 1. Tissue cross-sectional area as a function of nominal deformation. The cross-sectional area of the white matter strips ($n = 5$) decreased with increased compression as quantified by digital photographs taken during compression. Photographs are shown for 0%, 15%, 47%, 67%, and 80% nominal transverse compression. Clinically, neurological deficits are irreversible when spinal cord cross-sectional area is reduced by 65% (dashed line).

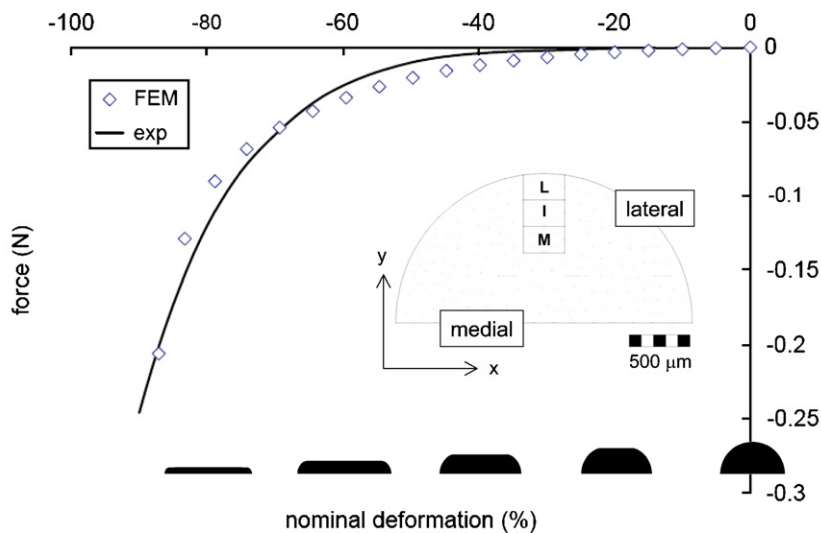


Fig. 2. Typical experimental (exp) and computational (FEM) force–deformation responses. The FEM geometry was derived from photographs taken during testing (Fig. 1). The finite element model consisted of 401 triangular elements. M, I, and L labels correspond to the medial, intermediate, and lateral regions sampled using the HRP exclusion test. The computational force–deformation response and deformed geometries were generated using material parameters $C_{10} = 540$ Pa and $C_{01} = 240$ Pa. The RMS error between experimental and computational curves for this typical case was 0.0091 N. Deformed finite element model geometries are shown for levels of 0%, 20%, 40%, 60%, and 80% nominal compression.

Bilston and Thibault (1996) fit the stress–strain response obtained for uniaxial tensile tests of human cervical spinal cords to a hyperelastic model formulated from an Ogden strain energy function, while previous efforts to computationally model the elastic response of the spinal cord parenchyma have assumed a state of linear elasticity (Ichihara et al., 2001, 2003; Ozawa et al., 2001). *In vitro* uniaxial tensile tests have been performed on spinal cord tissue and the tissue response described using linear elastic theory (Bilston and Thibault, 1996; Fiford and Bilston, 2005; Ichihara et al., 2001, 2003). However, linear elastic theory can only be applied to special cases of elasticity:

infinitesimal, reversible, rate-independent deformations that result in a linear force response (Lai et al., 1993).

White matter cellular damage was quantified using an HRP exclusion test. HRP labeling is a well-established technique to visualize membrane tears or disruptions and has been widely used to denote neuronal membrane disruption or poration in the spinal cord and brain trauma. Moreover, HRP labeling has been found to correlate well with axonal functional recovery, such as membrane potential repolarization (Pettus et al., 1994; Shi et al., 2000; Shi and Borgens, 2000; Shi et al., 2002; Shi and Pryor, 2002; Shi, 2004; Shi and Whitebone, 2006). In this

Table 1
The trend of HRP uptake density increased with increased nominal compression and with increased tissue depth

Nominal compression (%)	White matter region		
	Medial	Intermediate	Lateral
25	108 ± 121 ^{c,d,e}	25.2 ± 24.3 ^{d,e}	36.0 ± 29.5 ^{d,e}
50	631 ± 198 ^{a,b,c}	129 ± 116 ^{a,f,g}	67.4 ± 58.0 ^{b,f,g}
70	1560 ± 782 ^{a,b,d}	564 ± 318 ^{a,d,f}	283 ± 124 ^{b,d,f}
90	2220 ± 1810 ^c	1840 ± 1650 ^{e,g}	1340 ± 960 ^{e,g}

^aSignificant difference between medial and intermediate regions ($p < 0.05$).
^bSignificant difference between medial and lateral regions ($p < 0.05$).
^cSignificant difference between 25% and 50% nominal compression ($p < 0.05$).
^dSignificant difference between 25% and 70% nominal compression ($p < 0.05$).
^eSignificant difference between 25% and 90% nominal compression ($p < 0.05$).
^fSignificant difference between 50% and 70% nominal compression ($p < 0.05$).
^gSignificant difference between 50% and 90% nominal compression ($p < 0.05$).

Table 2
Correlations with HRP uptake density obtained using single and multiple regression analyses

Independent variable(s)	R^2	Independent variable(s)	R^2
$\sigma_x, \sigma_y, \sigma_z, \tau_{xy}$ ^a	0.945	σ_3	0.436
$\sigma_x, \sigma_y, \tau_{xy}$ ^a	0.934	von Mises stress	0.434
$\sigma_x, \sigma_y, \tau_z$ ^a	0.904	$\epsilon_y, \epsilon_{xy}$	0.428
σ_x, σ_y ^a	0.893	ϵ_y	0.422
$\sigma_y, \sigma_z, \tau_{xy}$ ^a	0.813	ϵ_3	0.421
$\sigma_1, \sigma_2, \sigma_3$ ^a	0.781	σ_1, σ_2	0.413
σ_2, σ_3 ^a	0.772	$\epsilon_x, \epsilon_{xy}$	0.329
σ_y, τ_{xy} ^a	0.635	ϵ_{xy}	0.328
$\sigma_x, \sigma_z, \tau_{xy}$	0.623	σ_z, τ_{xy}	0.254
$\epsilon_1, \epsilon_2, \epsilon_3$	0.593	σ_1	0.223
ϵ_2, ϵ_3	0.572	σ_x, τ_{xy}	0.168
$\epsilon_x, \epsilon_y, \epsilon_{xy}$	0.505	τ_{xy}	0.168
Strain energy density ^a	0.495	σ_x	0.088
ϵ_x, ϵ_y	0.486	σ_z	0.075
σ_1, σ_3	0.461	ϵ_1, ϵ_2	0.056
ϵ_1, ϵ_3	0.455	σ_2	0.021
σ_x, ϵ_z	0.441	ϵ_1	0.017
σ_y, σ_z	0.436	ϵ_x	0.005
σ_y	0.436	ϵ_2	0.005

^aRegression is statistically significant ($p < 0.05$).

study, HRP uptake was minimal for the control (normal, uninjured spinal cord axons). Following mechanical insult, HRP uptake increased significantly, indicating increased neuronal membrane permeability and, therefore, white matter cellular damage.

Stress fields induced by transverse compression have been described qualitatively by Blight (1988) and by Panjabi and White (1988). This study is the first to quantify

Table 3
Correlations with log-transformed percent HRP uptake density obtained using single and multiple regression analyses

Independent variable(s)	R^2
$\ln(\epsilon_x), \ln(\epsilon_y), \ln(\epsilon_{xy})$ ^a	0.917
$\ln(\epsilon_1), \ln(\epsilon_2), \ln(\epsilon_3)$ ^a	0.916
$\ln(\epsilon_x), \ln(\epsilon_y)$ ^a	0.913
$\ln(\epsilon_1), \ln(\epsilon_3)$ ^a	0.909
$\ln(\epsilon_2), \ln(\epsilon_3)$ ^a	0.847
$\ln(\epsilon_y), \ln(\epsilon_{xy})$ ^a	0.785
$\ln(\epsilon_3)$ ^a	0.731
$\ln(\epsilon_y)$ ^a	0.731
$\ln(\epsilon_x), \ln(\epsilon_{xy})$	0.574
$\ln(\epsilon_{xy})$ ^a	0.562
$\ln(\epsilon_1), \ln(\epsilon_2)$	0.324
$\ln(\epsilon_2)$	0.081
$\ln(\epsilon_1)$	0.035
$\ln(\epsilon_x)$	0.000

^aRegression is statistically significant ($p < 0.05$).

stress levels within the spinal cord parenchyma and the first to establish a statistical correlation between spinal cord white matter cellular damage and tissue-level stress. Moreover, a nonlinear relationship was established between white matter cellular damage and tissue-level strain. Based on the data presented, we conclude that white matter cellular damage is the consequence of an amalgamation of tissue-level stresses and strains rather than any single component of stress or strain. This phenomenon is consistent with the von Mises stress criterion, an established method used to predict failure in ductile materials.

Future work is required to elucidate the specific relationship between tissue-level stresses and strains and cellular-level injury mechanisms. A more thorough understanding of spinal cord injury mechanisms, including the advances in computational modeling presented in this study, will enhance the development of effective therapeutic strategies.

Conflict of interest

The authors have no conflicts of interest to disclose for this manuscript.

Acknowledgments

The authors wish to acknowledge support from the Purdue Research Foundation, Discovery Park at Purdue University, and the State of Indiana, as well as the technical contributions of Gary Leung.

References

Barenblatt, G.I., 1996. Scaling, Self-similarity, and Intermediate Asymptotics. Cambridge University Press, New York.
 Bilston, L.E., Thibault, L.E., 1996. The mechanical properties of the human cervical spinal cord *in vitro*. Annals of Biomedical Engineering 24, 67–74.
 Blight, A., 1988. Mechanical factors in experimental spinal cord injury. Journal of the American Paraplegia Society 11, 26–34.

- Fehlings, M.G., Skaf, G., 1998. A review of the pathophysiology of cervical spondylotic myelopathy with insights for potential novel mechanisms drawn from traumatic spinal cord injury. *Spine* 23, 2730–2737.
- Fiford, R.J., Bilston, L.E., 2005. The mechanical properties of rat spinal cord *in vitro*. *Journal of Biomechanics* 38, 1509–1515.
- Glantz, S.A., 2002. *Primer of Biostatistics*. McGraw-Hill Medical Publishing Division, New York.
- Henderson, F.C., Geddes, J.F., Vaccaro, A.R., Woodard, E., Berry, K.J., Benzel, E.C., 2005. Stretch-associated injury in cervical spondylotic myelopathy: new concept and review. *Neurosurgery* 56, 1101–1113.
- Ichihara, K., Taguchi, T., Shimada, Y., Sakuramoto, I., Kawano, S., Kawai, S., 2001. Gray matter of the bovine cervical spinal cord is mechanically more rigid and fragile than the white matter. *Journal of Neurotrauma* 18, 361–367.
- Ichihara, K., Taguchi, T., Sakuramoto, I., Kawano, S., Kawai, S., 2003. Mechanism of the spinal cord injury and the cervical spondylotic myelopathy: new approach based on the mechanical features of the spinal cord white and gray matter. *Journal of Neurosurgery* 99, 278–285.
- Kraus, K.H., 1996. The pathophysiology of spinal cord injury and its clinical implications. *Seminars in Veterinary Medicine and Surgery—Small Animal* 11, 201–207.
- Lai, W.M., Rubin, D., Krempl, E., 1993. *Introduction to Continuum Mechanics*. Pergamon Press, Oxford, NY.
- Ozawa, H., Matsumoto, T., Ohashi, T., Sato, M., Kokubun, S., 2001. Comparison of spinal cord gray matter and white matter softness: measurement by pipette aspiration method. *Journal of Neurosurgery* 95, 221–224.
- Panjabi, M., White, A., 1988. Biomechanics of nonacute cervical spinal cord trauma. *Spine* 13, 838–842.
- Pettus, E.H., Christman, C.W., Giebel, M.L., Povlishock, J.T., 1994. Traumatically induced altered membrane permeability: its relationship to traumatically induced reactive axonal change. *Journal of Neurotrauma* 11, 507–522.
- Shi, R., 2004. The dynamics of axolemmal disruption in guinea pig spinal cord following compression. *Journal of Neurocytology* 33, 203–211.
- Shi, R., Blight, A.R., 1996. Compression injury of mammalian spinal cord *in vitro* and the dynamics of action potential conduction failure. *Journal of Neurophysiology* 76, 1572–1580.
- Shi, R., Borgens, R.B., 2000. Anatomical repair of nerve membranes in crushed mammalian spinal cord with polyethylene glycol. *Journal of Neurocytology* 29, 633–643.
- Shi, R., Pryor, J.D., 2002. Pathological changes of isolated spinal cord axons in response to mechanical stretch. *Neuroscience* 110, 765–777.
- Shi, R., Whitebone, J., 2006. Conduction deficits and membrane disruption of spinal cord axons as a function of magnitude and rate of strain. *Journal of Neurophysiology* 95, 3384–3390.
- Shi, R., Asano, T., Vining, N.C., Blight, A.R., 2000. Control of membrane sealing in injured mammalian spinal cord axons. *Journal of Neurophysiology* 84, 1763–1769.
- Shi, R., Luo, J., Peasley, M.A., 2002. Acrolein inflicts axonal membrane disruption and conduction loss in isolated guinea pig spinal cord. *Neuroscience* 115, 337–340.